On High-Drag States of Nonlinear Stratified Flow over an Obstacle

J. T. BACMEISTER

Geophysical Fluid Dynamics Program

R. T. PIERREHUMBERT

Geophysical Fluid Dynamics Laboratory/NOAA, Princeton University, Princeton, New Jersey

(Manuscript received 10 April 1987, in final form 25 June 1987)

ABSTRACT

We have carried out a numerical investigation of the nature of high-drag states occurring in nonlinear stratified flow over obstacles. In particular, we consider the relative merits of theories which view the drag enhancement as due to linear resonance vs mechanisms which seek to exploit analogies with nonlinear hydraulic theory.

First we examine the behavior of the system as a function of the height of a zero-wind line imposed in the ambient flow. The character of the high-drag states conforms well to the predictions of the internal hydraulic analysis of Smith, and cannot be explained in terms of linear resonance. However, a high-drag state emerges even when the initial critical level height is below the lowest predicted resonant height. In this case an upstream-propagating bore is generated which adjusts conditions so as to allow a high-drag state. Further experiments with a narrow mountain revealed that nonhydrostatic effects do not appreciably affect the behavior for the lowest resonant position, but considerably reduce drag at the higher order resonances.

In the second series of experiments, the numerical model is initialized with the idealized high-drag states yielded by Smith's theory, subject to uniform upstream wind conditions. When the mountain is high enough to produce wavebreaking in uniform flow, an overturning region develops at the theoretical level of no motion and a vertically propagating wave emerges aloft; nevertheless, the flow near the ground remains substantially unaltered. When the mountain is too low to support wavebreaking, the mixed region in the lee collapses, and the flow reverts to a nonhydraulic Long's model solution subject to a radiation upper boundary condition. Thus, wavebreaking is a crucial part of the dynamics maintaining the high-drag state.

Our results expose some aspects of nonlinear gravity wave critical level behavior that are of general interest. The long term properties of the critical level were found to depend on the phase of the incident wave. Of particular interest are the circumstances in which the critical level acts as an absorber for all time. In this case the convergence of vertical momentum flux is balanced by a divergence of horizontal momentum flux, a state of affairs which can occur only for a horizontally localized wave packet incident on a horizontally unbounded critical level.

1. Introduction

a. Overview: Wave-breaking and high-drag states

When a stratified current flows over an obstacle, the obstacle experiences a drag force. Predicting the dependence of this drag force on the various flow parameters is a problem of obvious interest. Although much of the work in this area has been motivated by the phenomenon of severe downslope windstorms, the results have consequences extending far beyond their application to this purely local mesoscale event. Apart from its general intellectual attractions as a fundamental problem in fluid dynamics, understanding the nonlinear drag behavior is central to any attempt to parameterize the effects of mountain drag on larger scale circulations.

Field observations and numerical experiments have revealed that in the nonlinear regime the drag can be an order of magnitude greater than that obtaining in linear theory or in the steady nonlinear theories of the type pioneered by Long (1972 and references therein). As a result of their work on the simulation of downslope windstorms Peltier and Clark (1979) were the first to perceive the important association between wave-breaking and high-drag states. In the high-drag configuration low level air parcels experience *permanent acceleration* as they cross the mountain, and do not return to their undisturbed far-upstream speed. Such asymmetric, high-drag flows have been observed in a variety of numerical models. Pierrehumbert and Wyman (1985) were apparently the first to establish that the far-upstream and downstream flow modifications, the hallmark of hydraulic behavior, can occur even in the absence of strong structure in the initial wind and static stability fields, provided there is wave breaking. Detailed numerical experiments exploring the utility of hydraulic theory when the oncoming flow has a strong inversion at low levels were carried out by Durran (1986). Smith (1985) presented a simple steady state theory that confirms the relevance of the hydraulic

Corresponding author address: Dr. Raymond T. Pierrehumbert, Geophysics Fluid Dynamics Laboratory, Princeton University, P.O. Box 308, Princeton, NJ 08542.

analogy for a wide variety of flows in which wave breaking occurs. Nevertheless, there is still considerable controversy surrounding the precise mechanism of the high-drag states. In this paper, we shall resolve a number of the major issues by means of a program of numerical experimentation. First, we provide a critical review of the two major viewpoints on the problem.

b. *Resonant amplification theory*

The idea advanced by Peltier and Clark (1979) is that the wavebreaking region aloft acts as a reflector, and that its altitude is arranged such that the space between the breaking layer and the ground is a resonant cavity for internal gravity waves. The resonance hypothesis was explored further by Clark and Peltier (1984; hereafter CP84), who studied the evolution of mountain waves propagating in an ambient flow which had a preexisting zero-wind line, a situation we shall refer to as the "environmental critical level case." This configuration, which is also the subject of much of the present work, is summarized in Fig. 1. This problem is of vital importance not only because of the prevalence of critical level flows in nature but also because the flow provides a stringent test of our understanding of nonlinear flow over mountains. Moreover, gravity wave critical level dynamics is of importance in countless phenomena besides the mountain wave problem which is the immediate motivation here.

The key result of CP84 is that the drag is a sensitive function of the height H_0 of the imposed critical level, with high-drag states occurring in the vicinity of a discrete set of preferred values of H_0. Their results are reproduced in Fig. 2. Work carried out independently by Tomine (1984) also showed that critical layer flow can lead to high drag. He found moreover that this effect could account for certain strong depressions observed in the lee of mountains in Hokkaido.

The theory proposed by CP for the preferred values of H_0 rests on three assumptions: 1) linear, hydrostatic theory captures the essence of the phenomenon, except in the vicinity of the critical level; 2) the critical level acts as a *perfect reflector* located at H_0; and 3) the phase of the reflection is such that the effective boundary

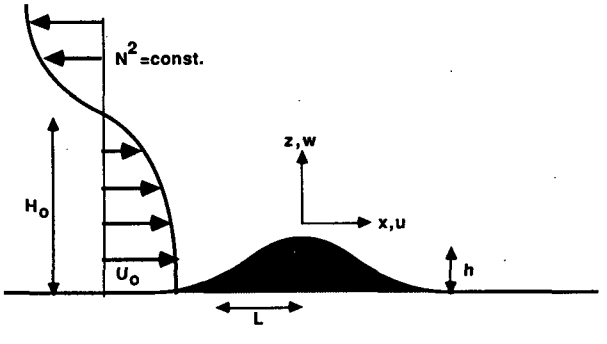

FIG. 1. Schematic of the geometry used in the critical layer experiments. Here N is the Brunt-Väisälä (stability) frequency.

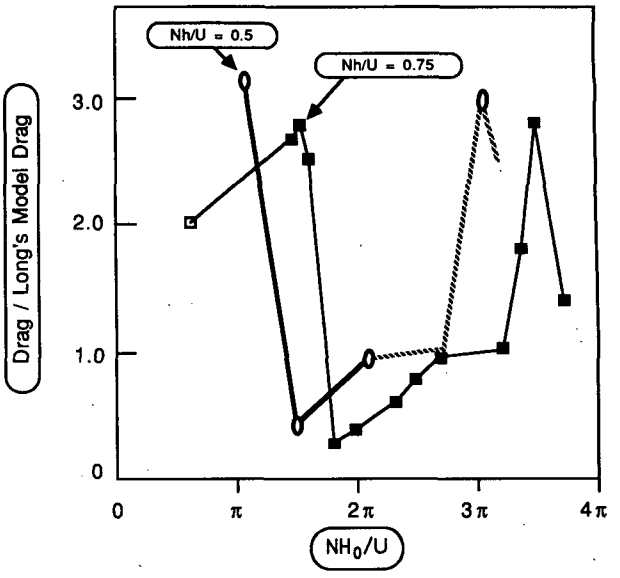

FIG. 2. Light line: Maximum surface drag as a function of critical layer height H_0 for flows over a mountain with $Nh/U_0 = 0.75$ (after Clark and Peltier, (1984)); filled squares are results taken from Clark and Peltier, while the open square is an additional data point added in the present study. Open circles: results from the present study, with $Nh/U_0 = 0.5$, showing that the position of the high-drag states shifts with mountain height; the dashed line connecting these results is a suggestion of what the detailed drag curve might look like for the lower mountain. The drags are normalized by the Long's model drag for uniform flow U_0 over an obstacle of the appropriate height, subject to a radiation upper-boundary condition.

condition is $\partial_z w = 0$ at $z = H_0$. Given these assumptions, the forced wave grows resonantly when $NH_0/U_0 = \pi/2, 3\pi/2, 5\pi/2, 7\pi/2 \cdots$, where U_0 is the constant wind well below the critical level and N is the ambient stability frequency. One obtains no resonances without the reflection assumption 2, and even assuming perfect reflection the position of the resonances depends entirely on the specification 3 of the phase of the reflection. Since CP gave no a priori justification for the latter two assumptions, their theory is incomplete. We shall see in section 2 that for some values of H_0 the critical level actually acts as an *absorber* for all times. Experiments were carried out by CP only for $Nh/U_0 = 0.75$, where h is the mountain height; for this mountain, the "predicted" resonance positions at $3\pi/2$ and $7\pi/2$ are verified by the nonlinear simulations. The predicted resonance at $5\pi/2$ is absent, and CP did not examine critical levels as low as $\pi/2$.

Under what circumstances does a gravity wave critical level reflect, and when it does, what is the phase of the reflection? For the case in which the critical layer dynamics is linear, Booker and Bretherton (1967) showed that the critical level does not reflect as long as its local Richardson number (Ri) exceeds ¼; for large Ri the critical level becomes a perfect absorber, and none of the incident wave is transmitted. (For Ri = O(1) there may still be a partial reflection of the in-

cident wave from regions of rapidly varying wind or stability *below* the critical level.) On account of linearity, the conclusions hold regardless of whether the source $h(x)$ is sinusoidal in a periodic domain or localized in an unbounded domain.

The Booker–Bretherton theory is of limited applicability to the highly nonlinear regime of concern in the present work. There have been a number of theoretical studies of nonlinear stratified critical levels (see Maslowe 1986), which have invariably concluded that the critical level ultimately becomes a perfect reflector if the viscosity is small (see especially Maslowe 1972). The utility of these theories for our purposes is severely compromised by the assumption that the incident wave is sinusoidal in x. Because the solvability conditions used to disambiguate the purely inviscid family of solutions rely crucially on a closed streamline topology peculiar to the periodic case, it is unlikely that the results carry over to a localized incident wave in a horizontally unbounded domain. There are further theoretical reasons to expect the latter case to be fundamentally different from the periodic case; these will be taken up in section 2d. The only theoretical attempt on the unbounded case was that of Margolis and Su (1978), which yielded only partial results. From their analysis, the most one can conclude is that for critical level flow over isolated topography there are no steady, inviscid, adiabatic solutions which are asymptotic to undisturbed flow far upstream; if the topography is modified so as to permit solutions, there is an infinite multiplicity of possible states, and no indication of which would be realized.

As Maslowe (1986) has pointed out, there have been few numerical studies of stratified critical levels, and none with state-of-the-art resolution. Such experiments, as there are (e.g., Breeding, 1971), generally indicate some nonlinear enhancement of reflectivity, but these too have for the most part been carried out for periodic waves. Thus, the inquiry initiated by Tomine (1984) and CP84, and carried further in the present work, serves to map out previously unexplored features of critical level dynamics.

c. *Hydraulic analogies*

The following presumes a familiarity with the basic theory of one-layer hydrostatic flow over an obstacle ("hydraulics"). Readers unfamiliar with the subject may wish to consult the review articles by Baines (1987) or Long (1972). For hydraulic flow, one can define a local wave speed $\pm\sqrt{gD}$ and a local Froude number $F = u/\sqrt{gD}$, where D is the local layer depth and u the local fluid velocity. One distinguishes the three basic flow categories shown in Fig. 3, according to the pattern of F. The "transitional flow" in Fig. 3 is characterized by high drag and large winds in the lee. From time to time investigators have sought to connect transitional hydraulic states with severe downslope windstorms, but until recently, such attempts have foundered because it was not possible to identify a clear analogue of the interface height or of F in naturally occurring continuously stratified flows.

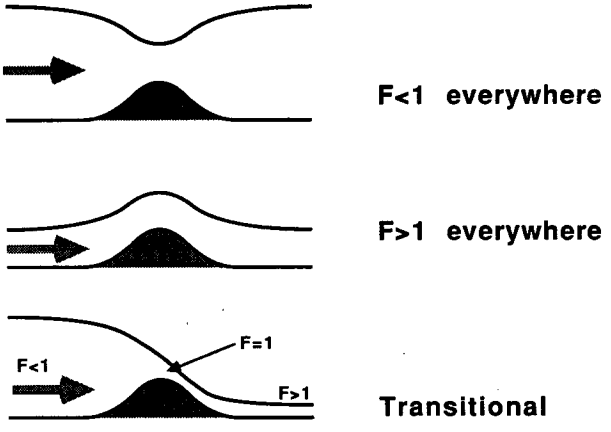

FIG. 3. Schematic behavior of one-layer hydraulic flow: top, subcritical; middle, supercritical; bottom, transitional.

While a complete generalization of hydraulic theory to continuously stratified flow has not yet been achieved, it has become clear that the essential ingredients necessary for a hydraulic analogy to hold are (a) a wave system which is nondispersive in the horizontal, and (b) a reflecting upper boundary condition (which need not be applied along a fixed, level surface). The former condition assures that a local wave speed can be determined at each x without reference to the state of the system elsewhere, while the latter discretizes the spectrum of wave speeds and vertically confines the wave energy put into the system. Small departures from the idealized conditions, e.g., a slightly leaky upper boundary or weak dispersion, can be tolerated. The interplay of the two conditions is illustrated most clearly in the asymptotic theory of Grimshaw and Smythe (1986), who solved the weakly nonlinear problem of flow of a continuously stratified fluid over a low obstacle when the oncoming flow is slightly detuned from an internal wave resonance. The numerical simulations carried out by Durran (1986) demonstrated that the hydraulic analogy holds over a broader range of conditions than that covered by the Grimshaw–Smythe theory.

The nondispersive condition is satisfied if the mountain is broad enough for the hydrostatic approximation to be valid. It is the identification of a suitable reflecting structure that has proved problematic in attempts to apply the hydraulic analogy to naturally occurring flow in the atmosphere. Similarly, in the context of the environmental critical level case, the fundamental issue is whether the critical level acts as a reflector. Even when it does, predictions cannot be made on the basis of the hydraulic analogy unless one has a theory for the phase of the reflections.

The key insight in Smith (1985) is the identification of a reflecting structure common to a wide variety of high-drag states observed in nature and in numerical models. Smith's theory rests on the assumption that there is a "dividing streamline" at height $H + \delta_c(x)$ above which the fluid is essentially quiescent, and that the density of the fluid between δ_c and H is well mixed; it is presumed that $\delta_c < 0$ and $\delta_c \to 0$ as $x \to -\infty$. Hydrostatic balance then implies the reflecting boundary condition $\partial_z \delta(x, z) = 0$ at $z = H + \delta_c(x)$, where δ is the streamline displacement. If the wind and static stability under the dividing streamline are uniform far upstream of the obstacle, then the exact nonlinear solution for the steady state flow below the dividing streamline can be obtained analytically using Long's model (Long, 1972). Given these assumptions the dividing streamline height is determined by the transcendental equation

$$h(x) = \delta_c(x) \cos[(N/U)(H + \delta_c(x) - h(x))], \quad (1.1)$$

which is analogous to the Benjamin-Lighthill cubic equation obtained in the 1-layer case (Long 1972). In (1.1) N is the far-upstream stability frequency and U is the far-upstream current. As discussed by Smith, (1.1) predicts that there is a discrete set of H for which transitional flow can occur, provided $Nh/U < 1$. The system is invariant under the transformation $H \to H + 2\pi (U/N)$, but unlike linear resonance is *not* invariant under $H \to H + \pi (U/N)$.

In applying his theory to complex flows, Smith asserts that high-drag states evolve only when the wave-breaking level nearly matches one of the values of H for which transitional flow can occur; the definition of "nearly" here is outside the scope of Smith's theory. An environmental critical level constrains wave breaking to occur at or somewhat below the zero wind line, if the mountain is not too high; $H + \delta_c$ is therefore identified with the height of the critical line, and the far-upstream dividing streamline height H is consequently identified with the environmental critical line height H_0. One further identifies U with the ground level wind speed U_0 in the environmental critical line case. These identifications permit a prediction of the values of H_0 leading to high drag. It is evident that the path leading to this prediction involves a number of speculative physical assumptions. Numerical experiments to be detailed here probe the validity of these assumptions and map out aspects of the phenomenology which are not covered by steady state hydraulics. It will be seen that despite its potential shortcomings, Smith's theory has considerable explanatory power.

It is prudent to inquire as to whether the two theories of high drag states are really distinct; indeed, in the work of Grimshaw and Smythe it was shown that the evolution of a high-drag transitional flow begins with linear resonance. Additionally, the boundary condition $\partial_z \delta_c = 0$ derived by Smith is equivalent to the condition $\partial_z w = 0$ assumed arbitrarily by CP84. However, Smith's condition is applied at the *displaced* critical level, whereas that of CP84 is applied at the *fixed height* H_0 (and likewise the bottom boundary condition is applied at $z = 0$). The quintessentially nonlinear effects captured by hydraulic theory show up most starkly in its prediction for the spacing of the high-drag values of NH_0/U_0. Linear resonances occur at intervals of π, but nonetheless high-drag states occur only at intervals of 2π because it is only for these values that the nonlinear feedback has the right sign to permit the resonance to evolve into a transitional flow.

d. *Outline of the paper*

In section 2, we describe a series of experiments in which a hyperbolic tangent wind profile with an environmental critical line is blown over mountains of various heights, and compare the results with the predictions of the resonant and hydraulic theories. Here, we also present momentum budgets which show how the wave pseudomomentum absorbed at the critical level affects the state of the large-scale flow. (See McIntyre 1981 for an explanation of why we do not speak of "wave momentum" in this context.) In section 3 the limits of Smith's theory as applied to flows with an environmental critical level will be tested, with particular emphasis on transient and nonhydrostatic effects. The importance of having an environmental critical line in the oncoming flow is examined in section 4, where experiments are described in which the ideal high-drag configuration postulated by Smith is used to initialize the time-dependent numerical model subject to *uniform* upstream flow.

Our principal conclusions are summarized in section 5. The results supporting these conclusions are culled from several dozen numerical experiments. It has only been possible to include the bare minimum of results needed to support our argument. In most cases, more complete results, particularly contour maps of flow fields and time dependences of drag, may be found in Bacmeister 1987.

2. Experiments with an environmental critical layer

a. *Overview*

The numerical experiments discussed here follow closely those described in Clark and Peltier (1984). A hyperbolic tangent wind profile is used:

$$U(z) = U_0 \tanh[(z - H_0)/\Delta] \quad (2.1)$$

where $\Delta = (U_0/N)$.

Further than Δ away from the critical line the mean wind can be regarded as constant with a value of U_0. These parameters give a minimum Richardson number of 1.0, which is somewhat lower than the value 2.25 used by CP84.

Our experiments were conducted with a conventional nonhydrostatic pressure-velocity model in ter-

rain following coordinates, similar to that employed by Clark (1977). The hyperbolic tangent mean wind is established from a state of rest with a body force applied for a sufficiently long time and then turned off. The flow is accelerated over a period of several advection times, L/U_0. The domain is periodic in the horizontal with a lateral sponge layer to absorb horizontally propagating disturbances. The wind in the lateral sponge layer is relaxed to the hyperbolic tangent profile. Further details concerning the model and initialization procedure may be found in Bacmeister (1987).

In these experiments, we found that the vertical resolution needed to provide satisfactory accuracy was surprisingly coarse given the fearsome reputation of critical layers. For several experiments Δz was varied from $0.33U_0/N$ to $0.12U_0/N$ without producing noticeable changes in the solution. It appears that the length scales which must be resolved are the shear thickness and the wave-induced parcel displacements in the breaking region. The first of these is externally imposed and the second is on the order of twice the mountain height in the experiments in question. The thickness of the nonlinear critical layer increases with the forcing amplitude, so we are left with the rather curious result that strong nonlinearity makes the phenomenon easier to resolve. The majority of the experiments described here were performed with a vertical resolution of $z = 0.25U_0/N$. The horizontal resolution was fixed at $x = 0.167L$ where L is the mountain half-width. In most of the experiments, 150 points were used in the horizontal and 40 points in the vertical. A vertical sponge of 12 points was found adequate to absorb the small amount of wave energy that was transmitted through the critical level.

In reporting our results, times will be measured in advection units L/U_0, lengths in units of mountain half-width L, depths in stratification units U_0/N and drag forces in units of U_0^3/N. The nondimensional parameters controlling the problem are Nh/U_0, NL/U_0, NH_0/U_0, and $\mathrm{Ri} = N^2\Delta^2/U_0^2$. A summary of the experiments referred to in this paper, together with the resulting drag, is given in Table 1.

b. *Numerical results*

1) PARAMETERS USED BY PELTIER AND CLARK

First, we would like to show briefly that the model used in this study is capable of reproducing the results of Peltier and Clark when similar parameters are used.

The mountain used in CP84 had $Nh/U_0 = 0.75$ and $NL/U_0 = 7.5$, and a high-drag state was found to evolve for a critical level height $H_0 = 3\pi/2(U_0/N)$. We carried out a simulation with $Nh/U_0 = 0.75$ and $NL/U_0 = 8.0$ for the same critical level height. Good agreement was found, both in the magnitude of the maximum surface drag and in the time behavior of the drag.

The potential temperature and velocity fields for this case are also much as found by CP84. At later times the critical layer flow is similar to the asymmetric hydraulic flows discussed in section 1. A relatively shallow layer of high winds is found at the surface. It is capped by a well-mixed, stagnant region that extends to the critical level. The smaller Ri at the critical level does

TABLE 1. Drag results for the numerical simulations discussed in this paper. Note: h is the mountain height, H_0 the critical layer or dividing streamline height, L the mountain half-width and Ri the Richardson number. In critical layer cases, U_0 is the magnitude of the wind far below the critical level; in cases initialized with the idealized steady states, U_0 is the far-upstream mean wind. Calculations performed with Ri = 1.0, except as otherwise noted. Drag reported in units of U_0^3/N. LM = Long's model; an asterisk, high-drag state (asymmetric hydraulic-type flow with downstream-propagating bore); lm, Long's model-type flow (absorbing critical layer); r, low-drag state (nonresonant reflecting critical layer).

Nh/U_0	NH_0/U_0	NL/U_0	Comments	D_∞
.75*	$3\pi/2$	8	D at $T = 28.13$	1.58
.5(r)	$3\pi/2$	8		<0.07
.5*	3.45	8		0.67 ± 0.03
.5*	$3.45 + 2\pi$	8	D still increasing at $T = 60$	0.56
.5(lm)	$3.45 + \pi$	8	Attains LM value by $T = 12$	0.21
.75*	2.0	8		1.05
.15(r)	0.7π	8		0.02
.15*	0.5π	8	D still increasing at $T = 22$	>0.04
.08*?	0.4π	8	D still increasing at $T = 22$	>0.0063
.5*	3.45	8	Ri = 10.89	0.42
.75*	$3\pi/2$	2		1.21
.5(r)	$3\pi/2$	2		<0.07
.5*	3.45	2		0.51 ± 0.05
.5*	$3.45 + 2\pi$	2		0.29 ± 0.05
.98*	$3\pi/2$	10	Initialized with theoretical solution	3.78
.5(lm?)	3.45	10	Initialized with theoretical solution	0.404
.98*	$3\pi/2$	4	Initialized with theoretical solution	3.0 ± 0.4

not appear to have had much effect on the evolution of the high-drag flow. Given the close agreement between the present results and those of CP84, we assume that our model has resolved the processes that caused the development of the high-drag configuration in CP84.

2) EXPERIMENTS WITH $Nh/U = 0.5$

For a mountain of height $Nh/U_0 = 0.75$, as used in CP84, Smith's theory predicts that the lowest value of H_0 yielding transitional flow is $4.1U_0/N$. This is close to the critical level height $3\pi/2U_0/N \approx 4.7U_0/N$ which CP84 found to give the largest surface drag. However, as the mountain height decreases towards zero, Smith's theory predicts that the first critical H_0 decreases to $\pi/2(U_0/N)$; for $Nh/U_0 = 0.5$, the theory predicts a high-drag regime for $H_0 = 3.45(U_0/N)$. On the other hand, the mechanism proposed by CP84 predicts no dependence on mountain height since it relies on linear resonance. It is, therefore, possible to distinguish between the two theories by extending the critical level experiments of CP84 to smaller mountain heights.

In Fig. 4 we show surface drag as a function of time for two flows over a mountain with $Nh/U_0 = 0.5$. The critical line is at $H_0 = 3.45(U_0/N)$ in one case and at $H_0 = 3\pi/2(U_0/N)$ in the other. The flow with $H_0 = 3.45(U_0/N)$ has a maximum surface drag that is twice as large as the largest surface drag for $H_0 = 3\pi/2(U_0/N)$. Furthermore, the drag in the "linear resonance" case drops precipitously after reaching its maximum

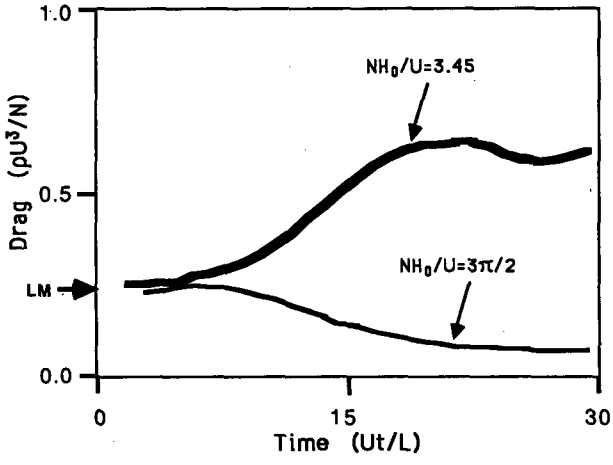

FIG. 4. Surface drag as a function of time for critical layer flow over a mountain of height $Nh/U_0 = 0.5$ and width $NL/U_0 = 8.0$. Results are shown for two critical line heights. The lower curve is obtained when $H_0 = 3\pi/2U_0/N$, the resonant value predicted by Clark and Peltier (1984). However, for the lower mountain, the drag decreases almost to zero after reaching a maximum value associated with freely propagating waves, the Long's model value. For $H_0 = 3.45U_0/N$ the drag increases well beyond the steady state value predicted by Long's model. For a mountain of $Nh/U_0 = 0.5$, a critical line height of $3.45U_0/N$ is consistent with an asymmetric state in the nonlinear resonance theory of Smith (1985).

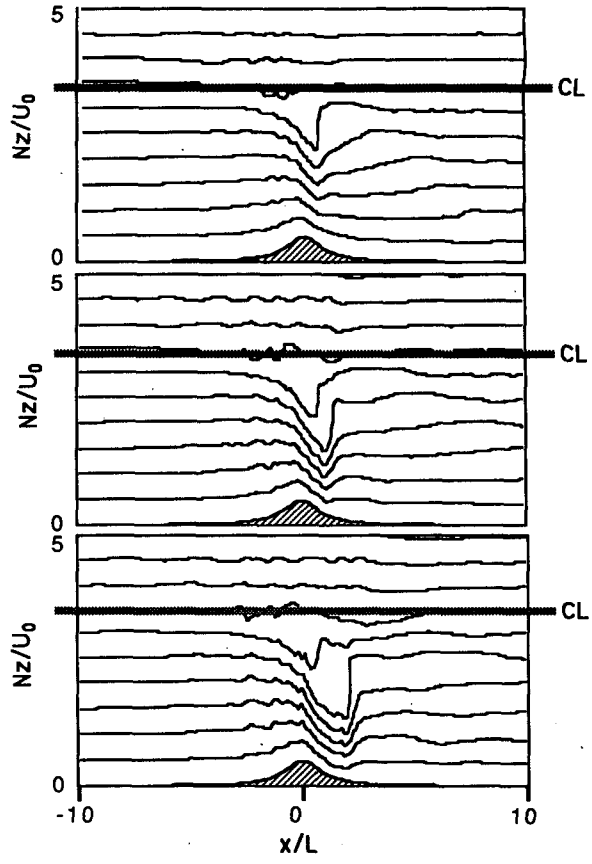

FIG. 5. The θ fields for a mountain with $Nh/U_0 = 0.5$ and $NL/U_0 = 8.0$ and a critical line height of $H_0 = 3.45U_0/N$. Top panel: $t = 9L/U_0$; middle panel: $t = 13.5L/U_0$; lower panel: $t = 18L/U_0$. This asymmetric pattern is characteristic of the high-drag state.

value near $t = 5L/U$. The maximum value is close to the steady state momentum flux predicted for this topography by Long's model subject to a radiation boundary condition, which is shown for comparison in Fig. 4. In contrast, when $H_0 = 3.45(U_0/N)$, the drag continues to increase right up to the end of the integration.

Potential temperature fields from the experiment with $Nh/U_0 = 0.5$ and $H_0 = 3.45(U_0/N)$ are shown in Fig. 5. Results for $H_0 = 3\pi/2(U_0/N)$ are shown in Fig. 6. A distinct difference between the flows is evident at later times. The flow with the critical level at $H_0 = 3.45(U_0/N)$ evolves into an asymmetric configuration that strongly resembles the high-drag hydraulic states found in CP84. On the other hand, the flow with the critical level at the CP84 resonance position does not develop this pronounced asymmetry. In fact, it becomes more symmetric as time progresses. The largest flow speeds occur aloft directly above the mountain, and in contrast to the high-drag case turbulent mixing is confined to a spot at the critical level directly above the mountain. The momentum flux for this experiment (not shown) approaches a steady state value of zero at

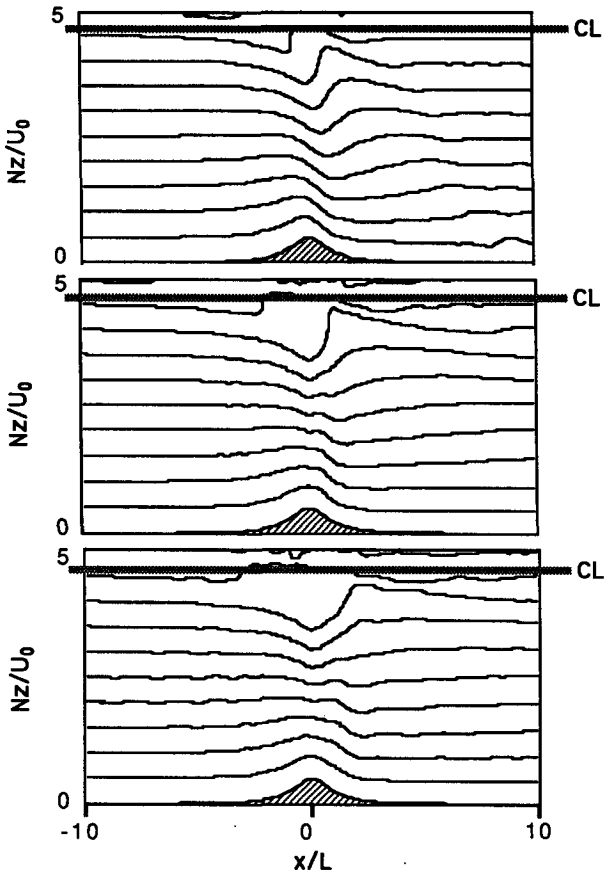

FIG. 6. The θ fields for a mountain with $Nh/U_0 = 0.5$ and $NL/U_0 = 8.0$ and a critical line height of $H_0 = (3\pi/2)U_0/N$. Top panel: $t = 9L/U_0$; middle panel: $t = 18L/U$; bottom panel: $t = 28L/U_0$. This pattern is characteristic of the low-drag state, in which the critical level acts as a nonresonant reflector.

all levels, suggesting that a vertically trapped mode is the dominant flow feature.

Both the time history of the drag and the final state attained imply that when $H_0 = (3\pi/2)U_0/N$, the critical line acts as a perfect reflector located at a nonresonant height. Although Smith (1985) claimed validity for his theory only for high-drag transitional flow, it is of interest to determine whether his upper boundary condition remains valid for nonresonant reflection. To estimate the phase of the reflection, we apply Long's model below the critical level. The steady solution is

$$\delta = h(x)\cos[(N/U_0)(z - h)] + A(x)\sin[(N/U_0)(z - h)], \quad (2.2)$$

where A is determined by the upper boundary condition applied at $H_0 + \delta_c(x)$. From Fig. 6 we estimate $\delta_c = -0.5$ at the mountain crest; application of the boundary condition $\partial_z\delta = 0$ implies $A = 0.64h$, whence (2.2) predicts a node in δ at $z = 2.64$. This is in excellent agreement with the node at $z = 2.7$ in Fig. 6.

3) HIGHER-ORDER RESONANCES

In order to examine the spacing of the resonances two additional experiments with $Nh/U_0 = 0.5$ were performed. One is for a critical level at $H_0 = (3.45 + \pi)U_0/N$ and the other for $H_0 = (3.45 + 2\pi)U_0/N$; final drags for these two cases may be found in Table 1. Only the latter develops into a high-drag state, confirming the spacing of $2\pi U_0/N$ between the resonances predicted by Smith's formulation. Examination of the wind and θ fields confirms also that the flow develops into a transitional state with high surface winds in the lee of the mountain much as in Fig. 6. This takes much longer than it did in the cases with critical lines below $3\pi/2U_0/N$. By $60L/U_0$, the surface winds are 75% as strong as the maximum winds in the case with $H_0 = 3.45U_0/N$. However, at the end of the integration, surface winds are still increasing.

For $H_0 = (3.45 + \pi)U_0/N$ no anomalous growth in the surface drag occurs. The flow patterns for this experiment (Fig. 7), do not show the pronounced upstream–downstream asymmetry that is seen in the high-drag flows. However, the flow does not approach the symmetric modal structure, characteristic of perfect nonresonant reflection, seen in Fig. 6. At the end of the integration, the structure below the critical layer still resembles that of a vertically propagating wave train in a vertically unbounded domain. This impression is reinforced by the momentum flux profiles, which become uniform in z, up to the critical level. The value of the vertical momentum flux below the critical level approaches the value in Long's model for the same topography. In contrast to the situation depicted in Fig. 6, where the critical level becomes a reflector, in Fig. 7 the critical level remains an absorber throughout

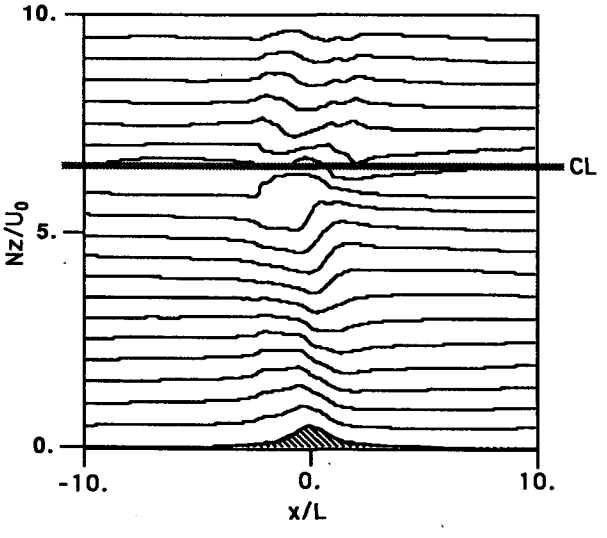

FIG. 7. The θ field for $Nh/U_0 = 0.5$ and $H_0 = (3.45 + \pi)U_0/N$ at time $t = 40L/U$. This pattern is characteristic of the "absorbing state" in which the drag has the value appropriate to Long's model subject to a radiation upper boundary condition.

the calculation. This reveals the subtlety of the nonlinear critical level dynamics: evidently, the reflection and absorption coefficients depend on the phase of the incident wave. There is as yet no analytical theory of this phenomenon.

Our drag results for the lower mountain are plotted, together with those of CP84 in Fig. 2. The drags are normalized by Long's model drag for uniform flow U_0 over an obstacle of the appropriate height, subject to a radiation upper boundary condition. It is clear that reducing the mountain height leads to an overall shift to the left of the high-drag values of H_0, much as predicted by the hydraulic theory. We see also that the results of CP84 support our finding that the nonlinear critical layer is an absorber when H_0 is about a half wavelength above the peak drag position. Their calculations exhibit a plateau in which the drag is close to the value obtained in Long's model for a mountain with $Nh/U_0 = 0.75$ and $NL/U_0 = 7.5$.

The reflective boundary condition incorporated into (1.1) cannot, of course, lead to an absorbing state; in the "odd order resonance" case (1.1) predicts the emergence of an exactly symmetrical zero drag state similar to the nonresonant reflecting case shown in Fig. 5; e.g., with $H_0 = (3.45 + \pi)U_0/N$ and $Nh/U_0 = 0.5$, the critical line displacement δ_c is symmetric about the obstacle and has maximum value +0.53 at the crest. Further insight can be obtained by considering the predictions of (1.1) for flow over a small mountain with H_0 set at an odd order linear resonance; in this instance, the detuning of the resonant cavity by displacement of the reflecting structure causes the wave amplitude to saturate at $O(h^{1/2})$, but the response remains symmetric rather than transitional, owing to the sign of the displacement. This state of affairs is a novel possibility in internal hydraulic theory, which has no counterpart in the one-layer case. Such symmetric states no doubt come to pass when the upper boundary assures reflection (e.g., if $N^2 = 0$ aloft), but the critical level need not always act as a reflector. A fully predictive theory of the drag must await a better understanding of the appropriate boundary condition to apply at a nonlinear critical level.

c. *Comparison with steady states postulated in Smith (1985)*

The strong dependence of surface drag on mountain height suggests that the analysis presented in Smith (1985) is substantially correct. Further evidence of this comes from a comparison of the flow fields in the numerical experiments with those obtained from the ideal configuration of Smith (1985). The idealized flow patterns can be readily computed from the formulas given in Smith's paper. Note that the environmental critical level does not appear explicitly in these flows. It is assumed that its effects can be completely subsumed into the specification of the dividing streamline height.

In Fig. 8 we show the idealized horizontal velocity and potential temperature fields for transitional flows over a mountain with $Nh/U_0 = 0.5$. Above the dividing streamline height, H_0, uniform stratification and constant horizontal wind with a speed U_0 have been assumed. Ignoring the downstream-propagating jump present in the time-dependent flows, we see that there are strong similarities between the ideal steady states and the flows in Fig. 5. The time-dependent fields are much noisier due to the generation of small scales as waves break at the critical layers. Small-scale noise is also generated along the upper edge of the high wind layer in the lee, presumably by poorly resolved shear instability. The time-dependent flows show evidence of flow blocking upstream of the obstacle. This is not present in the ideal steady states, and probably results from the fact that initially the breaking level in the time-dependent flows is slightly below H_0. As will be discussed in 3b, an upstream propagating surge adjusts the incoming flow so that an asymmetric transitional steady state is possible.

However, the overall structure of the idealized asymmetric flows agrees with that of the time-dependent flows. According to (1.1) any transitional solutions for mountains with $h \to 0$ far upstream and far downstream must have $H_0 + \delta_c = \pi/2 + 2\pi j$ downstream of the mountain. The flow from the time-dependent numerical simulation shown in Fig. 5 satisfies this condition, approximately, with $j = 0$; the layer of strong flow capped by a mixed region has a depth of about $1.6U_0/N$ in the lee of the mountain.

The maximum flow speeds downwind of the mountain are somewhat weaker in the time-dependent results. The "dead" region on the other hand is not completely stagnant in the time-dependent flows as it is in

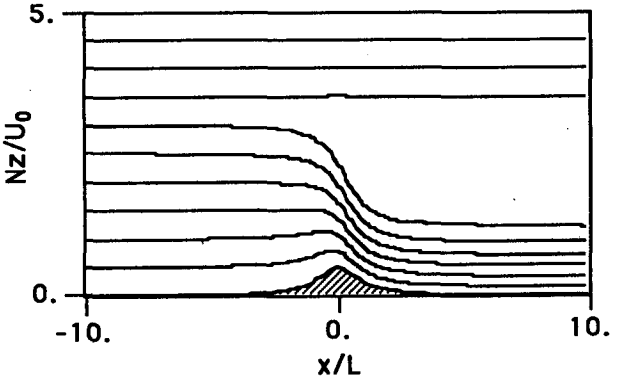

FIG. 8. Potential temperature field from ideal steady states postulated in Smith (1985). The solution is shown for $Nh/U = 0.5$ and $H_0 = 3.45U/N$. Contours are as in Fig. 5. Note that the difference in the level of the isentropes upstream and downstream of the mountain is well reproduced.

the idealized configuration. Several factors could contribute to the discrepancies. First, the flow below the dividing streamline in the numerical experiments does not exactly satisfy the conditions needed to apply Long's model, both because of its time-dependence and height-dependence. Upstream influence may reduce the average wind speed ahead of the mountain, and also cause its profile to deviate from the uniform flow required for Long's model. Second, the interface between the strong flow in the lee and the overlying "dead" region is a site of a large amount of turbulent mixing. This mixing vertically redistributes momentum between the strong flow layer and the dead region aloft. Last, the maximum winds in time-dependent simulations were still increasing slowly when the integrations ended, so that the final steady-state value may be closer to that predicted by Smith.

d. *Momentum budget*

According to Smith (1985) the surface drag in the idealized flows is given by

$$D = (H_0 - \pi/2)^3 U_0^3/6N. \qquad (2.3)$$

Smith's theory implies $H_0 = 3.45U_0/N$ and $H_0 = 4.1U_0/N$ for $Nh/U_0 = 0.5$ and $Nh/U_0 = 0.75$, respectively. This results in surface drags of $0.97U_0^3/N$ for $Nh/U_0 = 0.5$, and $2.5U_0^3/N$ for $Nh/U_0 = 0.75$. Both values are somewhat larger than those obtained for the same mountain height in the numerical experiments. The weaker lee surface winds in the time-dependent flows are consistent with the reduced drag, since they would also be associated with a smaller pressure drop across the mountain.

The ideal asymmetric flow configuration implies a large drop in horizontal momentum flux across the mountain. The momentum flux above the dividing streamline is identically zero, yet at the surface a large drag is exerted on the mountain. In the ideal flow, viscous fluxes and time-dependent terms are zero everywhere, so that this imbalance must be exactly compensated by a divergence of inviscid horizontal momentum flux.

Results of momentum budget calculations for several critical level flows are shown in Fig. 9. The momentum budget has been carried out for a box with sides at $x = \pm 4.0L$ and with a top at the critical line height H_0. The horizontal momentum fluxes are $\pm\int [\rho_0 u^2/2 + p]dz$, while the vertical flux is $\int \rho_0 uwdx$, the integrals to be carried out over the appropriate sides of the box. In the high-drag cases the cross-mountain drop in inviscid horizontal momentum flux cancels the large difference between surface drag and the wave momentum flux aloft. Similar results have been obtained for *uniform* upstream flow in the wave-breaking regime (see Chap. 5, Bacmeister, 1987). Each of the terms in the momentum budget is individually much larger than the net inviscid momentum flux.

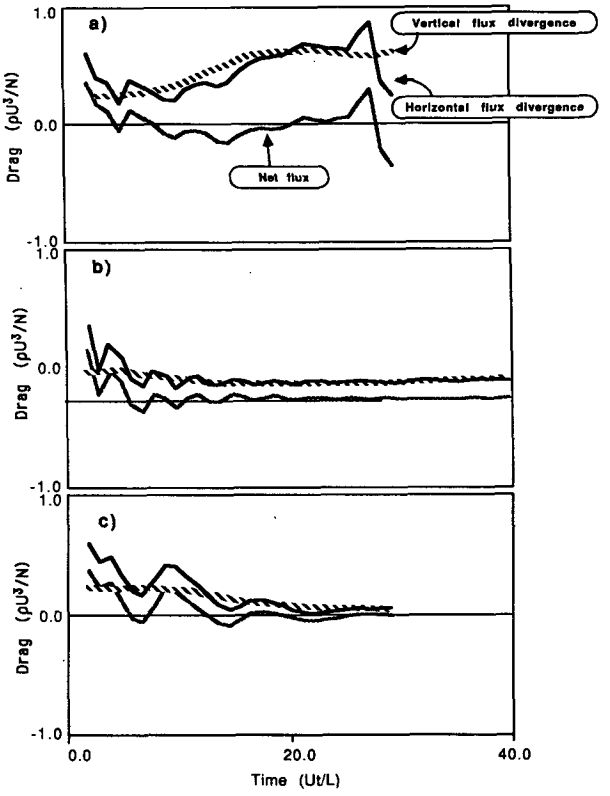

FIG. 9. Results of momentum budget calculations for a closed domain. The domain extends from $x = -4.0L$ to $x = 4.0L$ and from the surface to the critical line at H_0. Results are shown for (a) $Nh/U_0 = 0.5$, $H_0 = 3.45U_0/N$; (b) $Nh/U_0 = 0.5$, $H_0 = 3.45 + \pi U_0/N$; (c) $Nh/U_0 = 0.5$, $H_0 = 3\pi/2U_0/N$. In all cases $NL/U_0 = 8.0$. The plain curve in each panel represents the net inviscid momentum flux into the box. The remaining curves show the difference in horizontal momentum flux between -4.0 and $4.0L$, and the difference between the surface drag and the vertical momentum flux at $z = H$. In all cases, there is an approximate balance between horizontal and vertical divergence of momentum flux.

Budgets for two nonresonant cases are shown in panels B and C of Fig. 9. In the case with $Nh/U_0 = 0.5$ and $H_0 = 3\pi/2U_0/N$ the vertical momentum flux is near zero everywhere and the horizontal momentum flux appears to be nondivergent. However, the flow with $Nh/U_0 = 0.5$ and $H_0 = (3.45 + \pi)U_0/N$ has a momentum budget which is qualitatively similar to that of the resonant case (panel A), in which an appreciable, steady divergence of vertical momentum flux exists. This is balanced by a steady divergence of horizontal momentum flux. Thus, the critical layer behaves as an absorber of wave pseudomomentum, but not in the expected way. Little of the incident wave is absorbed locally by viscous processes, and at most a small fraction of its momentum flux goes into changing the flow locally. Rather, the incident wave is scattered

into horizontally propagating disturbances that create a drop in momentum flux across the obstacle.

The persistent absorbing states establish that the nonlinear evolution of a localized (in x) wave packet impinging on a critical level in a horizontally unbounded domain differs substantially from the horizontally periodic case. In the latter case the wave pseudomomentum absorbed at the critical level must show up as an order unity change in the x-averaged flow; as long as there is absorption, the mean flow must continue evolving and the system therefore cannot reach a steady state. In the unbounded case, the absorbed pseudomomentum can be carried away by horizontally propagating motions (such as the columnar modes discussed by Pierrehumbert and Wyman, 1985; Pierrehumbert and Bacmeister, 1987, in the uniform flow case), and in consequence the ambient flow where the wave packet encounters the critical level need not change much at all. Even the general results of Killworth and McIntyre (1985), which show that a barotropic Rossby wave critical level must in the mean act as a reflector, are inherently dependent on a periodic geometry. It is likely that in an unbounded domain, steady, absorbing Rossby wave critical levels could also exist.

3. Limits of the hydraulic approach

a. *Introduction*

The results of Smith (1985) are for steady, hydrostatic flow. Earlier we saw that in time-dependent flow over broad topography the theory yielded good results. Two questions arise immediately. The first concerns the influence nonhydrostatic motions may have on flows over narrower mountains. The resonance conditions could change, or asymmetric solutions could disappear altogether due to dispersion. These effects will be discussed in section 3. The second question concerns the sensitivity of the flow to small deviations of the position of the breaking level from resonance ("detuning"). According to Smith's theory, steady, asymmetric flows can exist only when the dividing streamline is exactly at one of the resonant positions. In practice, asymmetric flows appear when the breaking level is within some distance of the theoretical position. In 3b we will show that upstream influence can, in fact, lead to asymmetric flows even when the critical line is initially far below the theoretical resonance position.

A subtler question is whether Smith's reflecting boundary condition remains valid as the mountain height (and hence the thickness of the mixed region) decreases to zero. Assuming that it does, (1.1) predicts that a transitional flow configuration exists for arbitrarily low mountains. Numerical experiments addressing this point are described in section 3c.

Finally, there is the question of whether the linear partial reflections which are possible at finite Ri provide some of the vertical confinement needed in the hydraulic analogy. Experiments at large Ri are discussed in section 3d, and indicate that the partial reflections are unlikely to play a significant role.

b. *Upstream influence and sensitivity to critical line height*

1) ANALOGY WITH HYDRAULIC THEORY

A comparison of the flows in Fig. 5 with the ideal flow in Fig. 8 suggests that in the time-dependent experiments, the low-level flow upstream is somewhat weaker than in the idealized configuration. A quantitative comparison based on the wind data shows that in the time dependent flows the surface wind at $x \approx -2.0L$ is decelerated by as much as $0.3U_0$. In the ideal flows, however, the surface wind is not decelerated by more than $0.15U_0$.

In one-layer flow over an obstacle, an upstream surge is generated when the obstacle height is over the critical height needed to maintain a steady asymmetric solution. The surge decelerates the incoming flow and increases the depth of the layer. The new depth and flow are exactly those needed to maintain a steady asymmetric solution over the obstacle in question.

Guided by hydraulic theory we conjecture that asymmetric flows develop when the dividing streamline is at or below the theoretical resonant position for a given mountain. According to this view, the upstream influence observed in the time-dependent flows would result because breaking actually occurs somewhat below the environmental critical line. Upstream influence then corrects the resulting error in the height of the dividing streamline by adjusting N and U_0 appropriately. This conjecture can be tested by placing the zero wind line itself significantly below the lowest theoretical resonant position, H_0, for a given mountain. The analogy with hydraulic theory leads us to expect that an asymmetric flow will develop anyway, accompanied by strong modifications of the oncoming flow.

Figure 10 shows the time evolution of the upstream wind profile (at $x = -5L$) for an experiment in which $Nh/U_0 = 0.75$, and $NL/U_0 = 8.0$. According to theory, the lowest resonant dividing streamline height for this mountain is near $H_0 = 4.1U_0/N$. However, here the zero wind line has been imposed at $H_0 = 2.0U_0/N$. In Fig. 10 we see that a large upstream surge causes an adjustment in the horizontal velocity fields. The surface wind at $-5.0L$ has dropped to under $0.5U_0$ by the end of the integration, a 50% reduction; at $-2.0L$ the surface wind is near zero. The height of the zero wind line upstream of the mountain increases to 2.5 U_0/N. The strong blocking upstream is accompanied by strong surface winds in the lee. In Table 1 we see that the ultimate surface drag (plotted also in Fig. 2) is nearly twice that predicted by Long's model.

Thus, the analogy with hydraulic theory is at least partially correct. To be completely analogous the new upstream flow would have to satisfy the conditions for

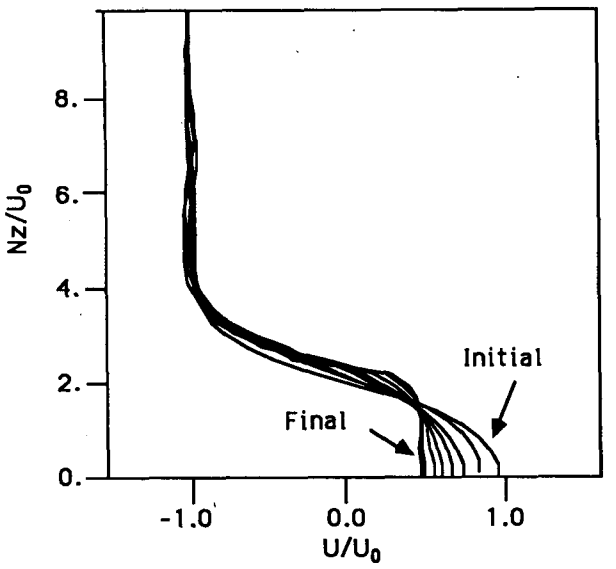

FIG. 10. Time evolution of upstream wind profiles $U(z)$ for a mountain with $Nh/U = 0.75$ and $NL/U = 8.0$ and a critical line height of $H_0 = 2.0U/N$. This value of H_0 is well below the minimum required for transitional flow in Smith's theory. The time ranges from $t = 0$ to $t = 28.2L/U_0$. Note the deceleration of the low-level flow as time progresses.

a steady asymmetric solution according to Smith's theory. When new nondimensional flow parameters are calculated, based on the far upstream conditions at $28L/U_0$ we see that the flow does, in fact, come somewhat closer to Smith's theoretical configuration. Denoting the final adjusted wind and stratification by U_f and N_f, we estimate a new mean wind, $U_f = 0.5U_0$, and stratification, $N_f = 0.75N$. The new nondimensional mountain height is $N_f h/U_f = 1.125$. The critical line, originally at $H_0 = 2.0U_0/N$, is shifted to $2.5U_0/N$. In terms of the new mean flow conditions this height becomes $3.75U_f/N_f$.

Smith's theory cannot accommodate mountains higher than $Nh/U_0 = 1.0$. He speculates that this dilemma may be resolved by upstream blocking which would effectively reduce the mountain height. In fact, a layer of nearly stagnant fluid exists at the foot of the mountain, which is still growing in the horizontal at the end of the integration. If the mountain height is measured from the top of this layer, a height in the range 0.5–$0.75N_f h/U_f$ results. With $H_0 = 3.75U_f/N_f$ a mountain of the reduced height yields reasonable agreement with Smith's prediction.

There are several reasons why the final state is not precisely like the idealized solution. First, the upstream wind has a tanh(z) profile. Since flow conditions are not initially uniform in z, Long's model equations, on which Smith's theory is based, do not hold exactly below H_0. This effect becomes more pronounced as the critical line is moved closer to the ground. Second, the upstream flow has not reached a steady state by the end of the experiment. The incoming flow at later times may approach closer agreement. Third, even if the upstream flow were initially uniform in height as required by Smith's theory, the upstream adjustment would introduce vertical shear in the oncoming flow. Despite these problems, the general level of agreement noted previously attests to the robustness of the hydraulic analogy.

2) BEHAVIOR FOR HIGHER-ORDER RESONANCES

The hydraulic analogy is not as successful for flows with critical lines far from the surface. Sufficiently strong upstream influence could always produce incoming flow consistent with an asymmetric state. Yet, this clearly does not happen in flows where breaking occurs just above the lowest resonant height, (see Fig. 6). Instead, the flow assumes an almost completely symmetric state resembling a subcritical solution in one-layer flow. When the critical line is above the lowest resonant height, H_0, the flow does not enter a high-drag configuration until the critical line is very close to the next resonant height. In the experiment with $H_0 = (3.45 + \pi)U_0/N$ and $Nh/U_0 = 0.5$ the zero wind line was initially $\pi U_0/N$ below the second resonant position at $H_0 = 3.45 + 2\pi U_0/N$. In that case the incoming flow did not adjust itself in a way that allowed an asymmetric configuration to develop. Clark and Peltier (1984) performed several experiments with critical lines between the first and second resonant positions. In Fig. 2 there is no evidence of resonant growth until $H_0 = 3.30U_0/N$, which is only $0.2\pi \approx 0.64U_0/N$ below the second resonance for $Nh/U_0 = 0.75$. Thus, there is evidence that when the critical line is above the lowest set of resonances, the breaking level must be close to the theoretical position obtained from steady state theory in order for a high-drag flow to develop. Although the steady states obtained by Smith are invariant to translations of the dividing streamline by $2\pi U_0/N$, time dependent flows with critical levels are not invariant under similar translations of the zero-wind line.

At this point, theory provides no clues as to when a transitional steady state may be expected to evolve in a time-dependent, critical layer flow. The phenomenology suggested by our simulations may be summarized as follows: Whenever the critical level is at or below the lowest resonant value for a given mountain height, an asymmetric high-drag hydraulic state develops, with the upstream flow adjusting, if necessary, to make the state possible. For higher resonances, however, the flow must be increasingly sharply tuned to the resonant conditions for the high-drag state to evolve. These conclusions presume that the mountain is not so high as to permit breaking to occur in the uniform flow conditions obtaining well below the critical level; when such low-level breaking can occur, the evolution of the high-drag state is unlikely to be appreciably influenced by the critical layer dynamics.

Some results pertinent to this regime will be discussed in section 4.

c. Small amplitude topography: Numerical results for $Nh/U = 0.15$ and $Nh/U = 0.08$

According to (1.1), the thickness of the stagnant region, $\delta_c(\infty)$ is $O(h^{1/2})$ for small mountains. Intuitively, we might expect that as it becomes thinner the flow will no longer feel the stagnant region as a reflecting upper boundary and the high-drag configuration would no longer form. Moreover for smaller mountains, linear critical dynamics (which yields absorption) remain valid for longer times, so that any resonant effects should set in later in the experiments.

Four experiments were performed with a mountain of height $Nh/U_0 = 0.15$ and width $NL/U_0 = 8.0$. The vertical resolution in these experiments was increased in order to resolve the wave displacements in the breaking region; a vertical grid length, $\Delta z = 0.08U_0/N$, was used. The computational domain had 80 points in the vertical. A sponge, 15 points deep, was sufficient to absorb the residual wave motion that managed to pass through the critical line. The horizontal resolution remained $\Delta x = 0.167L$. However, only 60 points were employed in the horizontal, with a lateral sponge 20 points wide. This restriction of the horizontal domain did not seem to affect the flow near the mountain during the relatively short integration periods used for these experiments.

Smith's theory gives a resonant H_0 of $0.797\pi U_0/N$ for a mountain with $Nh/U_0 = 0.15$. Numerical experiments with $H_0 = 0.8\pi$, 0.75π, 0.7π, and 0.5π times U_0/N were performed. Figure 11 shows histories of surface drag for two of these experiments. The drag does not significantly exceed the steady state value given by Long's model until $H_0 = 0.5\pi U_0/N$. The time history of drag for this value of H_0 is qualitatively different from that in the other cases. The evolution of the drag in the remaining experiments is similar to the one for $H_0 = 0.7\pi U_0/N$, which is also shown in Figure 11.

As suggested by linear critical layer dynamics, the high-drag flow with $Nh/U_0 = 0.15$ and $H_0 = 0.5\pi U_0/N$ evolves relatively slowly considering the height of the critical line. Its evolution should be compared with the evolution of the flow in the experiment with $Nh/U_0 = 0.75$ and $H_0 = 2.0U_0/N$. The critical lines are at similar heights. In the flow over the higher mountain, high-winds extend far to the lee by $9.4L/U_0$. For $Nh/U_0 = 0.15$, however, examination of the wind fields at $18.8L/U_0$ reveals that the high-wind layer is still confined near the mountain. The surface drag in the flow with $Nh/U_0 = 0.75$ and $H_0 = 2.0U_0/N$ begins to level off around $11.0L/U_0$. The surface drag in Fig. 11, on the other hand, grows steadily until the end of the integration at $22.5L/U_0$. Its magnitude doubles in about $15L/U_0$. Assuming a drop of $0.8U_0/N$ in the height of the dividing streamline across the mountain, we calculate a theoretical surface drag near $0.085U_0^3/N$ from (2.3). At $22.5L/U_0$ the drag in Fig. 11 has attained less than 50% of this magnitude. This is a further indication that the asymmetric configuration in this flow is still evolving.

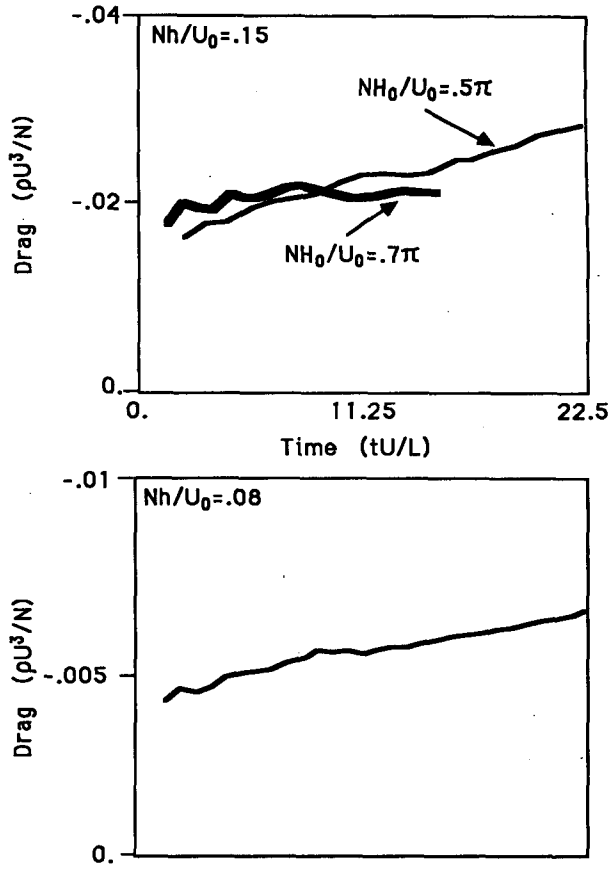

FIG. 11. Upper panel: surface drag as a function of time for flow over a mountain with $Nh/U_0 = 0.15$ and $NL/U_0 = 8.0$, with $H_0 = 0.7\pi U_0/N$ and $H_0 = 0.5\pi U_0/N$. Lower panel: results for $Nh/U_0 = 0.08$ with $H_0 = 0.4\pi U_0/N$.

Thus, a steady state configuration associated with high surface drag may exist for a mountain height of $Nh/U_0 = 0.15$. However, the time required for it to evolve is longer than was required for a more nonlinear flow with a critical line at a similar height. The fact that a resonance did not occur when H_0 was close to the theoretical value of $0.797U_0/N$ is probably a result of the z dependence of the mean wind profile. For small values of H_0 the wind changes significantly with height throughout most of the layer between the ground and the critical line. Long's model is no longer an accurate description of the flow below the dividing streamline, so that Smith's resonant heights may require modification. Increased phase change due to greater penetration of the wave into the region of weak wind (and consequently smaller vertical wavelength) may also play a role in modifying the effective upper boundary condition.

Resonant high-drag flows may develop for even smaller mountains. When $Nh/U_0 = 0.08$, a weakly asymmetric solution with steadily increasing drag occurs for $H_0 = 0.4\pi U_0/N$. The drag history for this experiment is shown in the lower panel of Fig. 11. We have found that the degree of asymmetry in the flow fields increases until the end of the integration, and the displacements at the critical line grow and the breaking region extends itself slowly downstream as time progresses. However, the flow fields are not as clearly associated with a high-drag configuration as those in the corresponding experiments with $Nh/U_0 = 0.15$. From Fig. 11, the doubling time for the surface drag for the lower mountain is about $45.0L/U_0$. The final surface drag is about 60% higher than that obtained in Long's model for a mountain with $Nh/U_0 = 0.08$ and $NL/U_0 = 8.0$. For a steady, high-drag flow over this mountain we obtain a drag of $0.02U_0^3/N$. The drag in Fig. 11 has reached only about 30% of this value by $22.5L/U_0$.

These results have not settled the question of whether there is a mountain height below which transitional high-drag flows cannot occur. Nevertheless, they do establish that the high-drag configuration takes longer to evolve as the mountain becomes smaller. This may result from the increasing penetration of the linear propagation zone into the shear layer as the wave amplitude decreases. Small amplitude waves can approach the zero-wind line more closely before overturning. Near the zero-wind line, the local, vertical group velocity decreases so that the time of propagation between the surface and the breaking region becomes longer. Moreover, when the mountain is small, it takes a longer time for nonlinear effects to change the critical level from an absorber to a reflector, though a reflecting state does ultimately emerge.

d. *Effects of shear layer thickness*

The propagation of linear gravity waves into a critical layer can be described with WKB theory as long as the minimum Richardson number in the shear layer is large. However, the mean flow with Ri = 1.0 used in the foregoing experiments may produce substantial partial reflections. It could be argued that this predisposes the flow toward hydraulic behavior. Here we will describe an experiment in which a much thicker shear layer is used.

The mean flow in this experiment is given by (2.1) with $\Delta = 3.3U_0/N$ and $H_0 = 3.45U_0/N$. The minimum Richardson number for the shear layer is given by $\text{Ri} = N^2/(U_0/\Delta)^2 = 10.89$. For this value of Ri, nearly complete absorption should occur in linear theory. The nondimensional height and width of the mountain used in the experiment are $Nh/U_0 = 0.5$ and $NL/U_0 = 8.0$, respectively. The mean flow speed between the critical layer and the surface is somewhat below $1.0U_0$, so that these values may be underestimates. However, to avoid confusion, quantities will continue to be scaled by the asymptotic wind, U_0.

The total surface drag for this flow increases throughout the integration, reaching a value slightly less than the Ri = 1.0 cases by the end of the integration (Table 1), which suggests that the flow is approaching an asymmetric high-drag state. The flow fields, (not shown), confirm this. Breaking occurs at lower levels than in the corresponding experiment with Ri = 1.0, (Fig. 5); however, this is to be expected since the average winds are weaker in the profile with Ri = 10.89. Other small differences between the flows arise from the fact that the mean wind is weaker when Ri = 10.89. First, the maximum drag and maximum surface winds are weaker here than they were in the corresponding case with Ri = 1.0. Second, the rate at which the surface drag grows is somewhat slower in terms of L/U_0 than it was in the case with Ri = 1.0.

Despite small modifications arising from the height dependence of the mean flow, the foregoing results imply that the parameters of the critical level are irrelevant to the dynamics of the high-drag configuration. As a corollary they imply that the interaction of a gravity wave with a stable, critical layer is dominated by strongly nonlinear processes that are independent of the mean flow Richardson number, at least when the mountain is not too small.

e. *Nonhydrostatic effects: Results for narrow mountains (NL/U = 2.0)*

The steady state theory in Smith (1985) is difficult to extend to nonhydrostatic flows due to the appearance of the ∂_{xx} terms in Long's model, precluding a local analytic solution at each x. A steady state solution with open lateral boundaries, a free nonlinear upper boundary, and a nonlinear bottom boundary would not be easy to obtain numerically either. A simple way to assess the importance of nonhydrostatic effects is to reduce the width of the mountain used in the simulations of critical layer flows.

The critical layer experiments discussed so far were for a broad mountain, $NL/U_0 = 8.0$, so that nonhydrostatic effects were unimportant for the larger-scale motions in the experiments. In order to assess nonhydrostatic effects, we performed several experiments with mountains having $NL/U_0 = 2.0$. Final drags for these experiments are given in Table 1. The first of this series had $Nh/U_0 = 0.75$ with a critical level at $H_0 = 3\pi/2(U_0/N)$. This arrangement of mountain height and critical layer height produced a large response with a broad mountain. This is again the case when $NL/U_0 = 2.0$. The maximum drag in this experiment is slightly smaller than it was in the corresponding experiment with $NL/U_0 = 8.0$. At the end of the integration it is still growing, however. The next two experiments had $Nh/U_0 = 0.5$. In one case the critical line is at $H_0 = 3.45U_0/N$ and in the other, at $H_0 = 3\pi/2(U_0/N)$. The

results follow the pattern observed for the broad mountain. A large response occurs in the surface drag for $H_0 = 3.45U_0/N$, while the drag for $H_0 = 3\pi/2(U_0/N)$ decreases almost to zero.

The high-drag flows in these experiments look similar to those obtained in the corresponding experiments with $NL/U_0 = 8.0$ (Fig. 5), except that there is some evidence that the downstream propagating jump in these flows begins to break up into small-scale nonhydrostatic oscillations, with wavelength on the order of $7.0U_0/N$.

The flow for the "nonresonant reflecting" case with $Nh/U_0 = 0.5$ and $H_0 = 3\pi/2(U_0/N)$ is more visibly affected by nonhydrostatic motion. The largest horizontal velocity over the mountain is only 60% as strong as it was in the corresponding case with $NL/U_0 = 8.0$. In the potential temperature field a train of small-scale waves is evident in the lee. These have approximately the wavelength obtained from linear theory for nondecaying lee waves in uniform flow with wind and stratification given by U_0 and N and a free-surface upper boundary near $z = 3\pi/2(U_0/N)$, further supporting the contention that in this regime the critical level acts as a free-surface reflector.

Overall, however, the modifications introduced by nonhydrostatic motion are minor when the critical line is low. In particular, the resonance structure derived from hydrostatic theory is unaffected.

When the critical layer is far from the surface, nonhydrostatic effects are more important. For a flow with $Nh/U_0 = 0.5$, $NL/U_0 = 2.0$, and $H_0 = (3.45 + 2\pi)U_0/N$, the surface drag does not show as dramatic an increase as it did in the corresponding experiment with $NL/U_0 = 8.0$ (See Table 1). Still, an excess of about 60% over the Long's model prediction occurs. Nonhydrostatic dispersion has significantly weakened the resonant response predicted by hydrostatic theory. However, there is still a distinct difference between this flow and a nonresonant flow such as the one obtained in the absorbing or reflecting regimes. This is borne out by the flow fields (not shown) which show the characteristic asymmetry between far-upstream and far-downstream flow conditions.

4. Importance of the environmental critical layer

a. Introduction

From the foregoing results, it is clear that the resonance structure predicted by Smith is correct for flows with an environmental critical line. However, the idealized high-drag configuration described in section 1c owes its existence to the upper boundary condition $\partial_z \delta_c = 0$. The key requirement for this condition is that the pressure along the upper branch of the dividing streamline, (i.e., $z = H_0$), be constant. The critical line flow favors this condition, as there is little transmission of wave energy aloft.

It is important to determine whether the presence of the critical line is crucial to the realization of the high-drag states. Next we will describe experiments in which the flow is initialized with the idealized high-drag configuration. In contrast to our previous experiments, constant wind and stratification will be imposed at the inflow boundary.

b. Experimental setup

The procedure used to introduce the idealized high-drag state into the numerical model is as follows. A large Rayleigh damping is added to the prognostic equations for u, w, and θ, that relaxes each field to the desired solution. The structure of the initial flow is given by Long's model once $\delta_c(x)$ has been determined numerically from (1.1), as in Smith (1985). The damping is left on long enough to allow any transients to die away, and then gradually turned off; a forcing period of $5.0L/U_0$ was found to be long enough.

Since the solutions are asymmetric between the far-upstream and far-downstream sides of the mountain, they must be modified before they can be introduced into a periodic domain. The supercritical solution in the lee must return to the upstream flow structure in a jump somewhere downstream of the mountain. If this jump is placed within the lateral sponge, it does not affect the flow in the interior in any way. This is the procedure we adopted.

The domain used in these experiments has 180 points in the horizontal and 40 points in the vertical. A lateral sponge, 60 gridlengths wide, is introduced to absorb horizontally propagating disturbances. The flow in the lateral sponge is relaxed to uniform parallel flow with constant stratification. The horizontal resolution is given by $\Delta x = 0.167L$. Although the flows studied imposed extreme variations across the lateral sponge, no significant reflection or generation of spurious waves occurred. The vertical resolution is $\Delta z = 0.33U_0/N$. A sponge, 12 gridpoints deep, is used below the top boundary. This was found adequate to absorb most of the vertically propagating wave energy generated during these flows.

c. Results

1) NEARLY HYDROSTATIC FLOWS ($NL/U_0 = 10.$)

Experiments were initialized with the ideal high-drag flows corresponding to $Nh/U_0 = 0.98$ and $Nh/U_0 = 0.5$. A mountain width of $NL/U_0 = 10.0$ was used. Flow fields for the case with $Nh/U_0 = 0.98$ are shown in Fig. 12. Instabilities can be seen to develop along the boundaries of the well-mixed region, but these weaken as the large shears are eliminated. The effect of these small-scale instabilities on the large-scale flow seems to be negligible. The surface winds in the lee of the mountain weaken quickly at the beginning, but reach a new steady value of $3.5U_0$. The surface drag (Fig. 14, lower panel) also weakens initially and then becomes relatively constant. Its final value is close to that obtained for a mountain of the same height when the

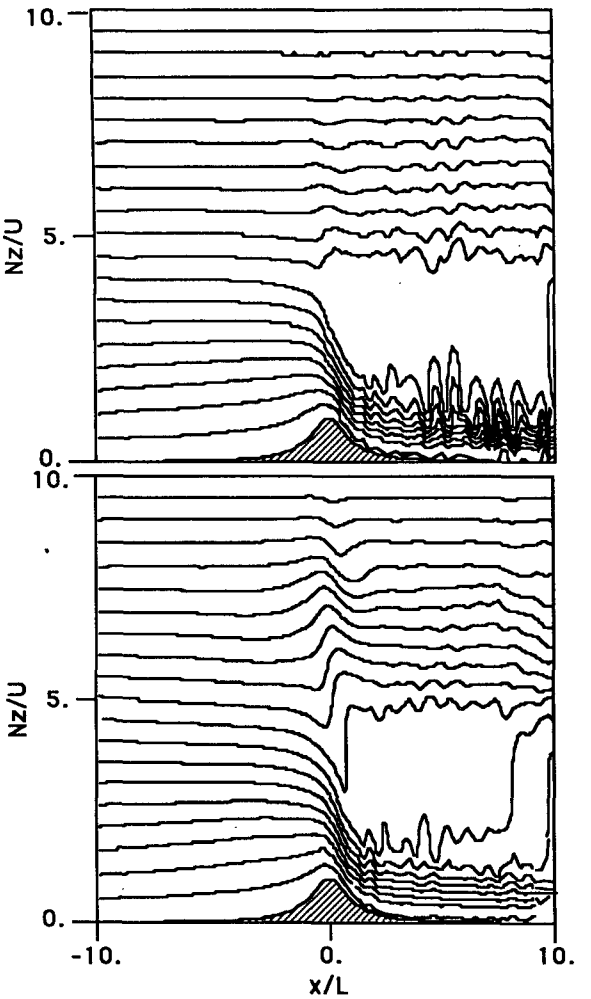

FIG. 12. Potential temperature fields from an experiment initialized with an ideal high-drag state such as the one pictured in Fig. 7. In this experiment a mountain with $Nh/U = 0.98$ and $NL/U = 10.0$ was used. The flow is shown at $t = 2.6$ and $15.0L/U$. A jump returns the flow to the structure it has upstream of the obstacle. In this experiment the jump is within the lateral sponge, and it remains steady throughout the integration.

flow is uniformly accelerated from rest [see panel A of Fig. V.15 in Bacmeister (1987)], and is comparable to the theoretical value given in (2.3).

The shape of the isentrope that marks the upper edge of the strong wind layer, called the critical isentrope hereafter, does not undergo any large changes. At the end of the integration it still drops from an upstream height near $z = 4.0U_0/N$ to a new level close to $z = 1.5U_0/N$ in the lee. However, the air aloft does not remain quiescent. Regions of overturning quickly appear above the mountain and persist throughout the integration. These waves produce an appreciable momentum flux aloft. The residual flux above $z = 5.0U_0/N$ becomes fairly constant with height and its value at the end of the integration is near $0.8U_0^3/N$. This is slightly below the saturated Long's model value for $NL/U_0 = 8.0$, which is about $0.9U_0^3/N$. The residual flux is far less than the surface drag, again implying considerable scattering of vertical into horizontal momentum flux in the breaking region.

The θ fields for $Nh/U_0 = 0.5$ are shown in Fig. 13, with drag history shown in the upper panel of Fig. 14. This mountain height is not sufficient to produce wave breaking in uniform flow, and the subsequent evolution away from the initial idealized state differs markedly from the previous case. The surface drag and lee surface winds decrease for the entire integration. The final value of the drag in this flow, $0.4U_0^3/N$, is well below $0.65U_0^3/N$, which is the largest drag obtained for the same mountain in the critical layer flows discussed in section 2. The potential temperature fields, shown in Fig. 13 confirm that the high-drag configuration is decaying. The shear between the windstorm and the stagnant region has weakened considerably by $25.0L/U_0$. The stagnant region no longer can be accurately described as such. The minimum flow speed near the mountain has increased to $0.3U_0$. The shape of the critical isentrope undergoes large changes. Its level in

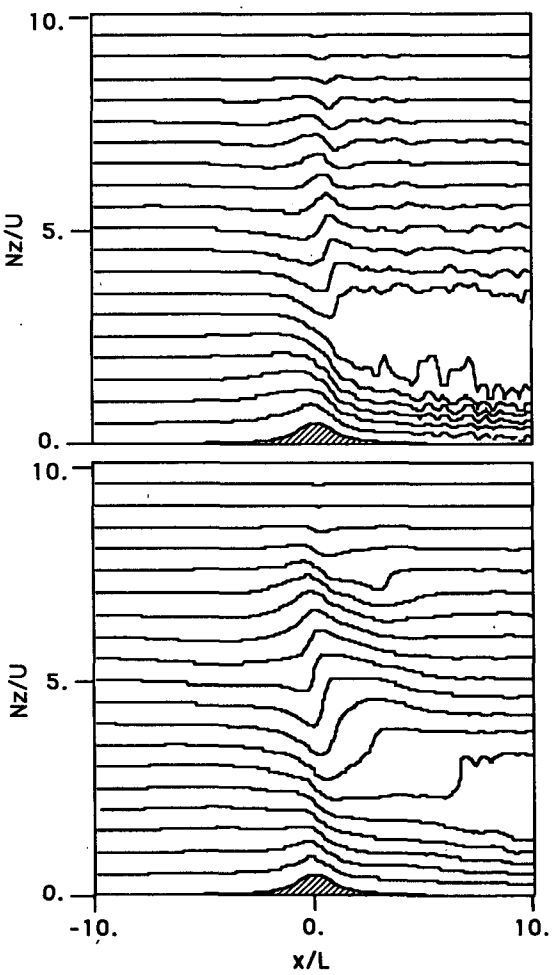

FIG. 13. As in Fig. 12, but for $Nh/U = 0.5$, a value that is too small to sustain wavebreaking in uniform flow.

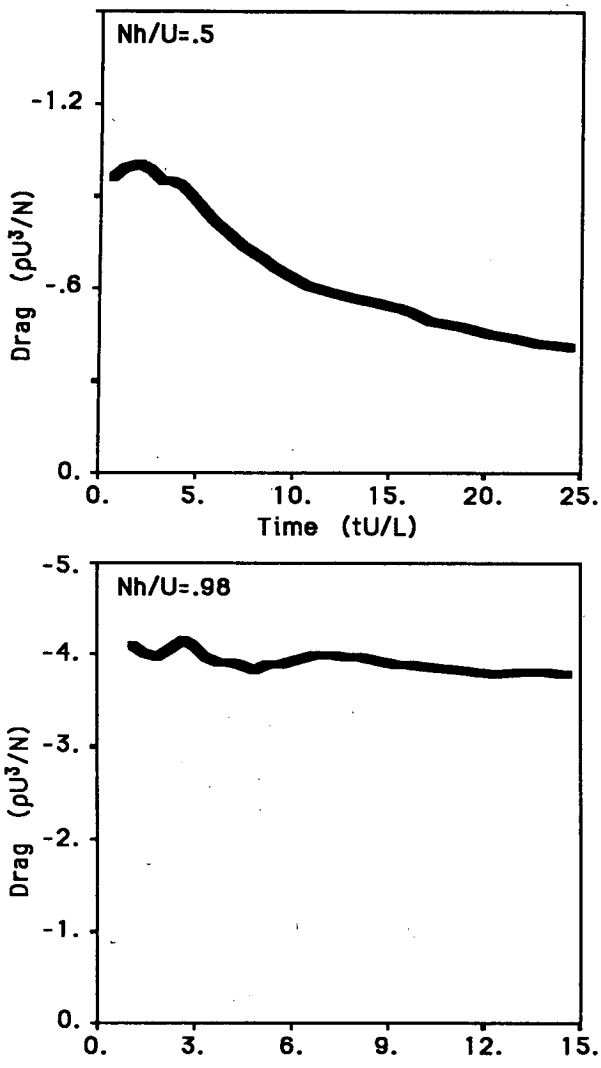

FIG. 14. Upper panel: surface drag vs time for $Nh/U = 0.5$, in the experiment initialized with the idealized steady state. The drag in this flow weakens significantly throughout the entire integration. Lower panel: surface drag vs time for $Nh/U = 0.98$, in the experiment initialized with the idealized steady state. After a quick decrease initially, the drag remains fairly constant until the end of the integration.

the lee of the mountain rises from $z = 1.5U_0/N$ to $z = 2.5U_0/N$.

The momentum flux profiles (not shown) approach a height-independent steady state. Interestingly, the drag and momentum flux aloft is around $0.4U_0^3/N$ at the end of the integration, which is substantially larger than the value of $0.2U_0^3/N$ obtained in Long's model for a mountain with $Nh/U_0 = 0.5$ and $NL/U_0 = 8.0$. This may be due to generation of transient gravity waves as the stagnant region undergoes wake collapse. Otherwise, the final flow above the mountain has a similar structure to solutions of Long's model.

From these results we conclude that Smith's ideal high-drag configuration is not a consistent steady state solution for flows with uniform conditions upstream. The upstream nose of the dead region is not stable. Soon after the start of the integrations the isentropes above the nose are drawn towards the surface. This perturbation grows rapidly and generates a significant amount of vertically propagating wave motion. The end effect of the instability is to allow the mountain wave train to propagate beyond the dead region. If the mountain waves do not induce overturning, the stagnant region cannot maintain itself indefinitely. It begins to collapse near the mountain. As it does, the flow below weakens.

Nevertheless, when wave breaking does occur, the flow below the breaking level remains close to the ideal configuration proposed in Smith (1985). This is true whether the breaking results because the mountain wave encounters a critical line or because the mountain is high enough to induce overturning in uniform flow. This suggests that wave breaking acts to produce a condition close to that postulated by Smith along the lower boundary of the breaking region.

2) RESULTS FOR $NL/U = 4$

As a further check on the robustness of the idealized hydraulic solutions, we have carried out an integration in a more nonhydrostatic regime. For $Nh/U_0 = 0.98$ with $NL/U_0 = 4$, the theoretical high drag state maintains itself much as it did in the case $NL/U_0 = 10$. In the narrow mountain case, the final drag is about $3U_0^3/N$, which is only slightly less than the $3.78U_0^3/N$ value found for the wider mountain (Table 1).

5. Summary and conclusions

a. Resonance structure: Conditions leading to high drag

Understanding the nature of motions forced by a mountain in a flow with wind reversal is of relevance to many naturally occurring flows, and, moreover, provides a challenging test of theories predicting effects of nonlinearity and wave breaking. The central datum a theory must explain is the dependence of drag on the critical level height H_0. Clark and Peltier (1984; henceforth CP84) attempt to explain their results in terms of resonant reflection from the critical line, though they do not provide any mathematical or physical argument to justify the assumed phase of the reflection. The internal hydraulic theory of Smith differs from this in providing a reflecting upper-boundary condition based on physical principals, and in capturing nonlinear effects associated with displacement of the reflecting surface. We have examined the relative merit of the two theories by means of numerical experimentation, and found the following.

For mountains above $Nh/U_0 \approx 0.7$, the theories of Smith (1985) and CP84 fortuitously yield similar predictions for the even-order "resonant" positions of a critical line. The experiments of CP84 were conducted with a mountain of $Nh/U_0 = 0.75$. In section 2b the work of CP84 was extended to include mountains of

lower heights. In contradiction with linear resonance theory, the response was found to depend dramatically on the mountain height. The shift of the resonance position was found to conform closely to that predicted in the nonlinear study of Smith (1985). A comparison of the flow fields in the numerical simulations with the ideal configuration revealed substantial quantitative similarity.

Also in accordance with Smith's theory, high drag transitional flow for $Nh/U_0 = 0.5$ was found when $NH_0/U_0 = 3.45 + 2\pi$, but not at $3.45 + \pi$. In the latter case, the critical level acts as an absorber for all time—a behavior which is outside the scope of Smith's calculation. Curiously, although the internal hydraulic equations with Smith's upper boundary condition yield a spurious reflecting state when applied to this case, they accurately reproduce the simulations of the "antiresonant" state found when H_0 is somewhat above the first high-drag position.

b. *Small amplitude topography*

The analysis of Smith (1985) predicts the possibility of a high-drag response for mountains of arbitrarily small height. In section 3c it was shown that in the presence of an environmental critical level, a transitional, high-drag flow can occur for mountains as small as $Nh/U = 0.08$. Thus, large amplitude incident waves are not needed to turn the critical level into a reflector. However, the time scale on which the drag evolves becomes longer as the mountain height decreases. It was speculated that this results because small waves can penetrate further into the critical layer, where the group velocity is small, before overturning.

For small mountains, Smith's equations do not accurately predict the critical line heights corresponding to high drag, suggesting that for lower amplitude incident waves, the phase of the reflection from the critical line differs from that yielded by Smith's physical argument.

c. *Hydraulic analogies for time-dependent flow*

Smith's analysis for the steady state in a high-drag flow has a clear affinity with results for steady one-layer flow over an obstacle. In section 3b we saw that this analogy extends at least partially to time-dependent flows in which the critical line is near the surface. It was shown that if the environmental critical line is initially below the position required by Smith (1985) for a steady, high-drag flow, the incoming flow is adjusted by a strong upstream surge. The critical line upstream of the mountain, is lifted, while the speed of the low-level flow is drastically reduced. The flow behind the surge has approximately the structure required for a steady, asymmetric state by Smith's theory.

When the critical line is above the first resonant height, the analogy with one-layer hydraulics breaks down for time-dependent flows. In any event, the implication is that a high drag state evolves when the critical level is *at or below* the lowest resonant dividing streamline height, or when it is *closely tuned* to one of the higher-order resonant positions. The general principle to be adduced from this is that the hydraulic analogy is most valid when the active layer is shallow enough that only a single vertical mode has the possibility of propagating upstream, and hence of becoming critical (i.e., stationary) at the mountain crest.

d. *Nonhydrostatic effects*

In section 3e it was shown that the predictions of Smith (1985) were not severely affected by nonhydrostatic motions when the critical line was near the surface. Experiments with a mountain of width $NL/U_0 = 2.0$ showed only minor differences from the nearly hydrostatic results when the critical line was below $H_0 = 3\pi/2U_0/N$. However, the resonant response for a critical line at $H_0 = (3.45 + 2\pi)U_0/N$ was significantly weakened. This has the obvious explanation that for higher H_0 the wave has more time to disperse in the horizontal before encountering the critical level.

e. *Importance of the environmental critical line*

Does the success of Smith's theory in the critical-level case carry over to the situation in which breaking occurs spontaneously in uniform ambient wind? In section 4, experiments were discussed in which ideal, high-drag flows were used as initial conditions for time-dependent, nonlinear simulations. The incoming flow in these experiments was uniform. We showed that the ideal, high-drag configuration is not a consistent steady state in the presence of uniform flow. Overturning was found necessary to maintain the stagnant region above the mountain. In cases where the mountain was too small to induce overturning, the stagnant region collapsed. Subsequently, the flow fields appear to be evolving toward the conventional Long's model solution, subject to a radiation upper-boundary condition. On the other hand, when the mountain was high enough to produce wave-breaking, Smith's idealized solutions were modified to the extent of producing an overturning region above the mountain near the dividing streamline height and a residual vertically propagating wave above this height, but the low-level flow remained substantially unchanged. From this we conclude that wave breaking serves not as an initial "trigger" forcing the flow to evolve into an alternate steady state, but it is a continuing and crucial part of the dynamics maintaining the high-drag state. This conclusion remains valid even in the moderately nonhydrostatic regime.

f. *Critical layer dynamics: General implications*

Although the present work was largely motivated by the problem of stratified flow over obstacles, a number of our results have implications in the broader context of general critical layer dynamics. In brief, we have

encountered three types of critical level behavior, depending on the phase of the incident wave: (a) The critical level acts as a perfect reflector, with the drag and vertical momentum flux falling to zero, and the flow assumes the perfectly symmetrical configuration characteristic of Long's model flow subject to a rigid-lid or free-surface upper boundary condition. (b) The critical level acts as a perfect absorber and the flow below it resembles a Long's model solution in a uniform current subject to a radiation upper boundary condition. (c) The critical layer acts as a reflector in accordance with Smith's upper-boundary condition, but the end state is an asymmetric transitional hydraulic flow involving large displacements of the critical level.

The transitional case is paradoxical: In order to derive the hydraulic theory, one must assume a reflecting upper boundary condition (though applied along a deformed surface). However, the profile of vertical momentum flux shows a decay with height that in other circumstances would be considered the hallmark of absorption. In fact, the momemtum budgets of cases b and c are similar in their essential character, with both exhibiting a balance between convergence of vertical momentum flux and divergence of horizontal momentum flux. Is the transitional flow case to be categorized as a reflecting or an absorbing critical layer? We are not certain that the distinction is meaningful, and prefer to characterize both b and c as scattering of vertically into horizontally propagating motions. Seen in this light, the chief difference between the two cases is the magnitude of the critical level displacement, and the main issue devolves to the efficiency of the horizontal radiation. When the horizontal radiation is less efficient, more of the incident wave pseudomomentum remains behind to cause large in situ changes in the flow. These novel aspects of critical layer behavior arise from the consideration of the behavior of a *horizontally localized* wave packet impinging on a critical level in a *horizontally unbounded* domain. Because of the possibility of a net convergence of horizontal momentum flux in this geometry, a convergence of vertical momentum flux can be supported in the steady state. This contrasts markedly with the behavior of Rossby wave critical levels in a periodic domain, as studied by Killworth and McIntyre (1985), which must ultimately become reflectors. Clearly, the whole subject of horizontally unbounded critical layers merits further investigation.

These issues of reflection vs absorption are of profound importance to any endeavor to parameterize the effects of gravity waves on larger scale circulations. A predictive theory of drag, and of momentum deposition due to diverse gravity wave sources must await resolution of the critical level issues raised here. Regardless of the upper boundary condition that ultimately proves appropriate, it is clear that nonlinear effects of the sort captured by hydraulic theory are of the essence.

Acknowledgments. This work has been submitted by JTB in partial fulfillment of the requirements for the degree of Doctor of Philosophy in the Program in Atmospheric and Oceanic Sciences, Princeton University. His support by a training grant from the National Aeronautic and Space Administration is gratefully acknowledged.

After the completion of the work reported on herein, the authors learned of recently completed calculations by Durran and Klemp which address some of the same issues as treated in section 2. Despite the use of an independent numerical model and somewhat different choices of parameters, their conclusions *vis-a-vis* the merits of the hydraulic analogy are, in every respect, consistent with ours.

REFERENCES

Bacmeister, J., 1987: Nonlinearity in transient, two-dimensional flow over topography. Ph.D. thesis, Princeton University, 187 pp.

Baines, P. G., 1987: Upstream blocking and airflow over mountains. *Ann. Rev. Fluid Mech.*, **19,** 75–97.

Booker, J. R., and F. P. Bretherton, 1967: The critical layer for internal gravity waves in a shear flow. *J. Fluid Mech.*, **32,** 513–539.

Breeding, R. J., 1971: A non-linear investigation of critical levels for internal atmospheric gravity waves. *J. Fluid Mech.*, **50,** 545–563.

Clark, T., 1977: A small scale dynamical model using a terrain following coordinate transformation. *J. Comput. Phys.*, **24,** 136–215.

——, and W. R. Peltier, 1984: Critical level reflection and the resonant growth of nonlinear mountain waves. *J. Atmos. Sci.*, **41,** 3122–3134.

Durran, D. R., 1986: Another look at downslope windstorms. Part I: On the development of analogs to supercritical flow in an infinitely deep, continuously stratified fluid. *J. Atmos. Sci.*, **43,** 2527–2543.

Grimshaw, R. H. J., and N. Smyth, 1986: Resonant flow of a stratified fluid over topography. *J. Fluid Mech.*, **169,** 429–464.

Killworth, P., and M. E. McIntyre, 1985: Do Rossby wave critical levels absorb, reflect or over-reflect? *J. Fluid Mech.*, **161,** 449–492.

Long, R. R., 1972: Finite amplitude disturbances in the flow of inviscid, rotating and stratified fluids over obstacles. *Ann. Rev. Fluid Mech.*, **4,** 69–92.

Margolis, S. B., and C. H. Su, 1978: Boundary-value problems in stratified flows with a nonlinear critical layer. *Phys. Fluids,* **21,** 1247–1259.

Maslowe, S. A., 1972: The generation of clear air turbulence by nonlinear waves. *Stud. Appl. Math.*, **51,** 1–16.

——, 1986: Critical layers in shear flows. *Ann. Rev. Fluid Mech.*, **18,** 405–432.

McIntyre, M. E., 1981: On the "wave-momentum" myth. *J. Fluid Mech.*, **106,** 331–345.

Peltier, W. R., and T. Clark, 1979: The evolution and stability of finite amplitude mountain waves. Part II: Surface wave drag and severe downslope windstorms. *J. Atmos. Sci.*, **36,** 1498–1529.

Pierrehumbert, R. T., and B. Wyman, 1985: Upstream effects of mesoscale mountains. *J. Atmos. Sci.*, **42,** 977–1003.

——, and J. T. Bacmeister, 1987: On the realizability of Long's Model solutions for nonlinear, stratified flow over an obstacle. *Proc. Third Int. Conf. on Stratified Flow, Pasadena.* Elsevier (in press.)

Smith, R. B., 1985: On severe downslope winds. *J. Atmos. Sci.*, **42,** 2597–2603.

Tomine, K., 1984: A numerical study on local depressions on the lee side of the Hidaka Mountain Range in Hokkaido. *J. Meteor. Soc. Japan,* **62,** 215–223.